

Generating Adversarial Events: A Motion-Aware Point Cloud Framework

Hongwei Ren, Youxin Jiang, Qifei Gu, Xiangqian Wu

Harbin Institute of Technology

Abstract

Event cameras have been widely adopted in safety-critical domains such as autonomous driving, robotics, and human-computer interaction. A pressing challenge arises from the vulnerability of deep neural networks to adversarial examples, which poses a significant threat to the reliability of event-based systems. Nevertheless, research into adversarial attacks on events is scarce. This is primarily due to the non-differentiable nature of mainstream event representations, which hinders the extension of gradient-based attack methods. In this paper, we propose MA-ADV, a novel **Motion-Aware Adversarial** framework. To the best of our knowledge, this is the first work to generate adversarial events by leveraging point cloud representations. MA-ADV accounts for high-frequency noise in events and employs a diffusion-based approach to smooth perturbations, while fully leveraging the spatial and temporal relationships among events. Finally, MA-ADV identifies the minimal-cost perturbation through a combination of sample-wise Adam optimization, iterative refinement, and binary search. Extensive experimental results validate that MA-ADV ensures a 100% attack success rate with minimal perturbation cost, and also demonstrate enhanced robustness against defenses, underscoring the critical security challenges facing future event-based perception systems.

1 Introduction

Deep Neural Networks (DNNs) have demonstrated exceptional performance across various domains, including Computer Vision (CV) and Natural Language Processing (NLP) [LeCun *et al.*, 2015]. However, despite these achievements, DNNs have been shown to be highly vulnerable to adversarial examples. By introducing imperceptible perturbations to the input data, adversaries can induce DNNs to produce erroneous predictions with high confidence [Xiang *et al.*, 2019], as shown in Fig. 1. This vulnerability raises significant concerns, particularly in safety-critical applications such as autonomous systems and robotics, where even minor mispredictions could have profound consequences. Adversarial ex-

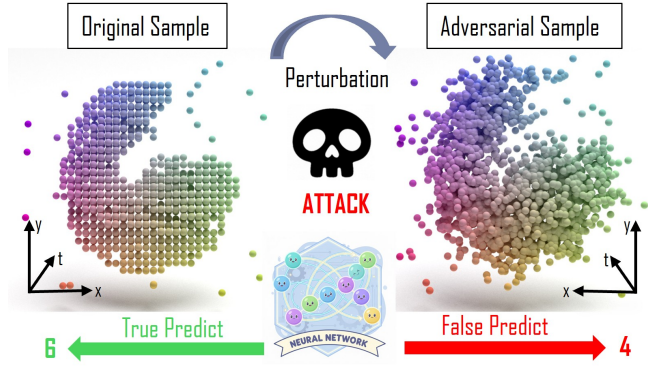


Figure 1: A representative adversarial example from the N-MNIST dataset. After the attack method adds perturbations to events, the network misclassifies the handwritten digit 6 as 4.

amples have been widely studied in various modalities such as 2D images, text, and 3D point clouds, with substantial efforts dedicated to enhancing the security and robustness of models [Zhang *et al.*, 2025]. Nevertheless, when it comes to event cameras, which operate differently due to their sparse and asynchronous nature, this research is still limited.

Event cameras, inspired by biological vision systems, offer a revolutionary approach to visual sensing by asynchronously recording pixel-level brightness changes at microsecond resolution [Gallego *et al.*, 2020]. Unlike traditional cameras that sample light intensity at fixed time intervals, event cameras respond to dynamic changes in the scene, allowing for continuous, high-speed data capture without redundant information. This capability, coupled with their high dynamic range and low latency, makes them well-suited for applications that require high temporal resolution, such as high-speed tracking and real-time robotics [Ren *et al.*, 2025a]. The raw events \mathcal{E} generated by event cameras are composed of four key elements: spatial coordinates (x, y) , precise timestamps t , and polarity p . However, the majority of research approaches stack raw events into frame-based representations for processing, making gradient-based adversarial sample generation impractical [Zhu *et al.*, 2018], primarily due to the non-differentiable nature of the data format transformation. This bottleneck hindered the development of adversarial events generation.

Point clouds, as a popular 3D representation, have seen

promise in the field of event cameras due to their capability to directly process raw events. Representative works include the utilization of PointNet++ [Qi *et al.*, 2017b] for tasks such as classification and segmentation, as well as EventMamba [Ren *et al.*, 2025b], which addresses the temporal discrepancies between events and point clouds, achieving remarkable performance in several tasks. Meanwhile, adversarial attacks on point clouds have grown in recent years, exploiting vulnerabilities and highlighting the need for robust defenses to ensure system reliability in real-world applications. For instance, classical adversarial attack strategies, such as IFGSM [Kurakin *et al.*, 2018] and C&W attacks [Xiang *et al.*, 2019], have demonstrated the potential to degrade the performance of point cloud recognition models by introducing subtle perturbations. Therefore, the adversarial strategies developed for point clouds offer valuable insights for the generation of adversarial samples in raw events.

Nevertheless, point cloud and events appear similar in their representation $((x, y, z) \text{ vs. } (x, y, t, p))$, the content they represent is fundamentally different [Ren *et al.*, 2023]. Point cloud attacks primarily target changes in geometric morphology and spatial structure, such as minimizing noticeable outlier points and coarse surfaces, which are perceptible features to the human eye [Lou *et al.*, 2024]. In contrast, events capture pixel-level brightness changes, encoding spatio-temporal information that reflects the dynamic trajectories and local motion trends of objects. Therefore, adversarial events generation should focus on attacking motion features while ensuring that the actual behavior of objects in the scene remains unchanged. Additionally, event cameras tend to generate numerous high-frequency noises due to the influence of hardware and the environment, which poses a challenge to the effective update of gradients. In this paper, we pioneer the generation of adversarial events from point cloud-based networks via perturbation. To begin with, we leverage the perturbation diffusion strategy to mitigate the high-frequency noise inherent in leveraging the weighted spatio-temporal neighborhood information of events, thus enhancing the stability of perturbation optimization during backpropagation. Furthermore, we adopt the sample-wise learning rate adjustment, which outperforms batch-wise one due to its ability to adapt to the inherent heterogeneity of individual samples and dynamically optimize the trade-off between attack success and perturbation cost. Our contribution can be summarized:

- We first design the gradient-based framework to generate adversarial events through the point cloud method.
- We implement perturbation diffusion across distinct events, incorporating the motion information.
- We adopt the sample-wise learning rate adjustment strategy to identify the optimal perturbations.
- Extensive experiments show MA-ADV not only maintains 100 % attack accuracy but also achieves the minimal cost.

2 Related Work

In this section, we systematically review the latest advances in adversarial attack methods for point cloud and events,

along with their key limitations and open challenges.

2.1 Point Cloud Adversarial Attack

A variety of classic gradient-based and perturbation-based adversarial attack methods have been developed for point cloud models. Initially, the gradient-based adversarial attack FGSM [Goodfellow *et al.*, 2014] was extended to the point cloud domain under an L_2 norm constraint and iterative variation [Liu *et al.*, 2019]. Subsequently, the C&W attack framework [Xiang *et al.*, 2019] was introduced to generate high-quality adversarial examples by shifting point coordinates, with the authors further proposing a method to achieve adversarial properties by adding individual points, point clusters, and entire objects. Beyond these addition-based strategies, a method was put forward to effectively cause misclassification in point cloud classification models by deleting a small number of high-saliency points [Zheng *et al.*, 2019].

As research advanced, point cloud attack methods began to evolve toward the goals of imperceptibility and smoothness. For example, the C&W framework was modified into a point-wise adversarial perturbation method for point clouds, which balances the magnitude of perturbations and the surface smoothness [Tsai *et al.*, 2020]. On the geometric optimization front, GeoA³ [Wen *et al.*, 2020] leverages the inherent geometric structures of data (e.g., manifold, distance, distribution characteristics) to generate adversarial examples. SI-ADV [Huang *et al.*, 2022] proposed the point cloud sensitivity map, a core tool that underpins both a powerful shape-invariant white-box attack and the first query-based black-box attack for point cloud recognition tasks. Manifold attack [Tang *et al.*, 2023] was also developed for 3D point clouds, which achieves attacks by explicitly perturbing the underlying surfaces of point cloud objects. In terms of balancing attack performance, HIT-ADV [Lou *et al.*, 2024] successfully struck a favorable trade-off between adversarial effectiveness and perturbation imperceptibility for target models. Finally, moving toward physically realistic attacks, SmokeAttack [Wei *et al.*, 2025] leverages Navier–Stokes-based smoke simulation to produce perturbations that are physically plausible for LiDAR systems. Despite the abundance of remarkable prior work, we argue that point clouds and events differ in their content properties, and thus the corresponding attack methods should place greater emphasis on spatio-temporal motion information.

2.2 Event Adversarial Attack

To date, research on generating event-based adversarial examples remains relatively limited. Early work leveraged projected gradient descent (PGD) to craft gradient-guided adversarial events by shifting the timestamps of original events and introducing null events [Lee and Myung, 2022]. However, this method only modifies a single dimension of events (time or existence) without modeling their spatio-temporal correlations, rendering the perturbations vulnerable to detection by defense mechanisms. Another white-box attack strategy, designed specifically for spiking convolutional neural networks, generates adversarial examples through event addition or removal [Büchel *et al.*, 2022], achieving high success rates with

minimal perturbation magnitudes on the N-MNIST and DVS-Gesture datasets. Nevertheless, this approach relies on manually designed perturbation rules and lacks effective modeling of event motion features, leading to significant sensitivity of attack success and limited generalization capabilities. More recently, physical adversarial attacks have been extended to event-based pedestrian detectors [Lin *et al.*, 2025], which frame the design of adversarial clothing textures as a 2D texture optimization problem. While this work does not directly modify raw event streams, it indirectly disrupts event generation via physical carriers.

In summary, these existing works merely adopt mature attack paradigms without redefining a gradient backpropagation framework tailored to the spatio-temporal characteristics of events. Furthermore, none addresses the high-frequency gradient noise inherent to the events' noise, nor do they implement mechanisms to stabilize the backpropagation process. These constitute critical gaps that our work aims to fill.

3 Preliminary

In this section, we formalize the problem setting of untargeted adversarial attacks on event streams, clarify the definition of events and attack objectives, and then review the fundamental gradient-based optimization methods for generating adversarial perturbations.

3.1 Problem Setting

Given a begin events stream $\mathcal{E} = \{e_n\}_{n=1}^N \in \mathbb{R}^{N \times 4}$, and each event $e_n = (x_n, y_n, t_n, p_n)$ is a 4-dimensional vector containing spatial coordinates (x, y) , a temporal t , and a polarity p information. A pretrained point cloud-based classifier $f(\cdot)$ can accurately predict its object-class label $Y = f(\mathcal{E}) \in \mathbb{R}^c$, where c is the total number of different classes. The goal of generating adversarial events on this victim classifier is to alter the benign event cloud \mathcal{E} into a perturbed one \mathcal{E}' , so that $f(\mathcal{E}') = Y'$ (targeted attack) or $f(\mathcal{E}') \neq Y$ (untargeted attack), where $Y' \in \mathbb{R}^c$ and $Y \neq Y'$. In this paper, the untargeted adversarial attack is explored by default, and we focus on perturbation-based attacks, which operate directly on the original events.

3.2 Gradient-based Method

The most commonly used method to generate perturbations is based on the gradient optimization algorithm. Specifically, in classic gradient-based adversarial attacks, perturbations are typically created by calculating the gradient of a classification loss with respect to the input raw events. The general formulation of this method can be expressed as an optimization problem subject to a distortion constraint.

$$\mathcal{L}_{\text{total}} = \mathcal{L}_{\text{cls}} + \lambda \cdot \mathcal{L}_{\text{distance}}(\mathcal{E}, \mathcal{E}') \quad (1)$$

$$\lambda_{j+1} = \text{BinSearch}(\lambda_j, \lambda_l, \lambda_h), j = 1, 2, 3, 4 \cdots J \quad (2)$$

Here, $\mathcal{L}_{\text{total}}$ represents the total loss function, which consists of the classification loss \mathcal{L}_{cls} (cross-entropy loss) and the distance loss $\mathcal{L}_{\text{distance}}(\mathcal{E}, \mathcal{E}')$ (such as L_2 distance) weighted by a balancing factor λ . A specific upper bound λ_h and lower bound λ_l are preset for λ , which is then searched for via the

binary search method [Xiang *et al.*, 2019]. Specifically, J denotes the total number of steps for the binary search process. Subsequently, adversarial events are generated by adding a small perturbation with fixed magnitude along the sign direction of the gradient of the model's loss function with respect to the input, as shown in the following formula:

$$\mathcal{E}' = \mathcal{E} + \epsilon \cdot g \quad (3)$$

$$g = \text{sign} \left(\frac{\partial \mathcal{L}_{\text{cls}}(f(\mathcal{E}), y)}{\partial f(\mathcal{E})} \cdot \frac{\partial f(\mathcal{E})}{\partial \mathcal{E}} + \lambda \cdot \frac{\partial \mathcal{L}_{\text{distance}}(\mathcal{E}, \mathcal{E}')}{\partial \mathcal{E}} \right) \quad (4)$$

where ϵ controls the magnitude of the perturbation, and the $\text{sign}(\cdot)$ function extracts the gradient direction to ensure perturbations are generated along the direction that maximizes the loss (FGSM). Furthermore, the mainstream approach tends to adopt an iterative method, while utilizing an optimizer to generate the perturbation, as described below:

$$\mathcal{E}_i = \mathcal{E} + \mathcal{P}_i, \quad i = 1, 2, \dots, I, \quad \mathcal{P}_0 \sim \mathcal{N}(0, \sigma^2) \quad (5)$$

$$g_i = \frac{\partial \mathcal{L}_{\text{cls}}(f(\mathcal{E}_i), y)}{\partial f(\mathcal{E}_i)} \cdot \frac{\partial f(\mathcal{E}_i)}{\partial \mathcal{P}_i} + \lambda \cdot \frac{\partial \mathcal{L}_{\text{distance}}(\mathcal{E}, \mathcal{E}_i)}{\partial \mathcal{P}_i} \quad (6)$$

$$\mathcal{P}_i = \text{Adam}(\mathcal{P}_{i-1}, g_i, \eta), \quad (7)$$

where I denotes the total number of iterations. \mathcal{P}_0 is the initial perturbation term, which is randomly initialized from a distribution \mathcal{N} with zero mean and variance σ^2 . The Adam optimizer updates the perturbation \mathcal{P}_i based on its previous iteration value \mathcal{P}_{i-1} , the current gradient g_i , and the learning rate η . Specifically, g_i is the gradient computed with respect to \mathcal{P}_i , combining the gradients of the classification loss and the distance loss from current input \mathcal{E}_i .

4 Method

In this section, we detail the design of the MA-ADV for generating adversarial events.

4.1 Motion-aware Perturbation Diffusion

Events often generate a large number of high-frequency noises, which are determined by ambient light and hardware noise. When these events are used in the process of gradient backpropagation, they will destabilize the attack process. The method of gradient diffusion can effectively suppress the interference of high-frequency noises and improve the stability of the backpropagation process. More importantly, during the diffusion process, the motion feature of the events should be taken into consideration, which can guide the gradient diffusion in the temporal and spatial domains and further enhance the model performance. The specific diffusion process will be elaborated upon below.

First, the K-Nearest Neighbor (KNN) method is employed to identify the spatial and temporal neighbors of each event. The spatial neighbors index \mathcal{I}_s and corresponding spatial distance set \mathcal{D} are obtained by retrieving the neighbors from raw events \mathcal{E} via the KNN algorithm. Meanwhile, the temporal neighbor index \mathcal{I}_t is derived by retrieving causal neighbors using the same KNN method. Specifically, both KNN_s and KNN_t utilize the combined distance of x , y , and t dimensions for grouping, with the key distinction

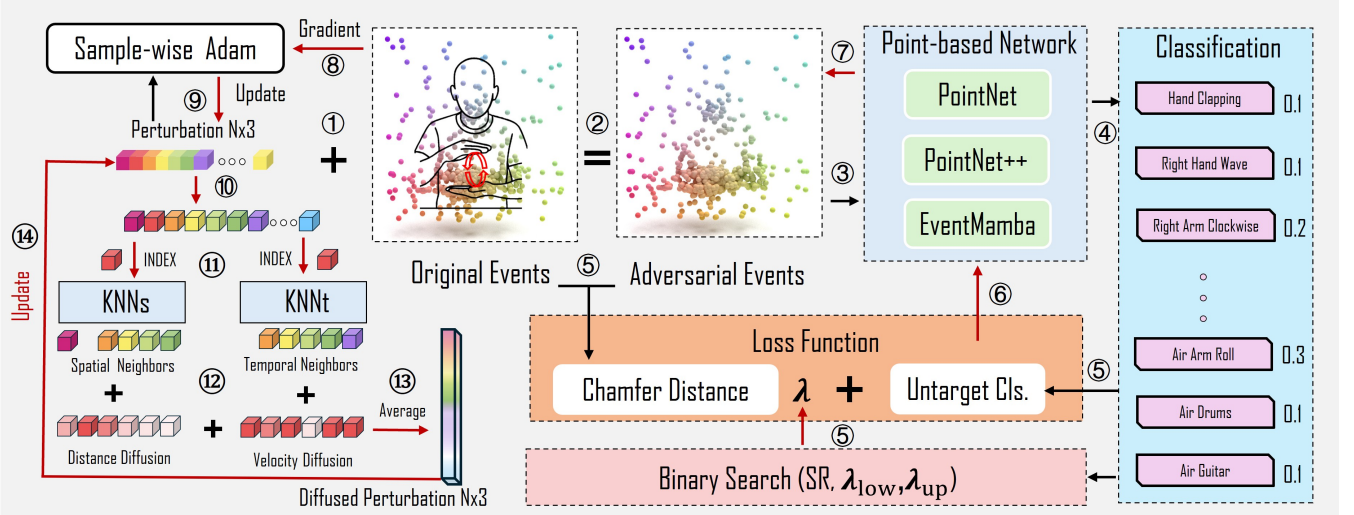


Figure 2: Overview of the MA-ADV adversarial attack framework. The method generates spatially and temporally consistent adversarial events by diffusing perturbations through spatial and temporal neighbors, which is optimized by a sample-wise Adam optimizer. The adversarial events are fed into point-based networks for classification, with the loss function balancing Chamfer Distance and an untargeted classification loss. Binary search dynamically adjusts the loss weight λ to optimize attack success rate and perturbation cost.

that KNN_t only selects the K samples generated after the current point to incorporate **causal relationships**, as shown in Fig. 2.

$$\mathcal{I}_s, \mathcal{D} = \text{KNN}_s(\mathcal{E}, K), \quad \mathcal{I}_t = \text{KNN}_t(\mathcal{E}, K). \quad (8)$$

Second, we define the diffusion process to execute the diffusion of each event's perturbation. For **motion feature**, we select velocity \mathcal{V} between events, which is derived from the x, y spatial coordinates and t timestamp of events, as shown below:

$$\mathcal{V}_i = \text{Norm}\left(\frac{\sqrt{(\mathcal{E}_n^x - \mathcal{E}_{n-1}^x)^2 + (\mathcal{E}_n^y - \mathcal{E}_{n-1}^y)^2}}{\mathcal{E}_n^t - \mathcal{E}_{n-1}^t}\right). \quad (9)$$

The numerator computes the Euclidean spatial distance between the n -th and $(n-1)$ -th events (where $\mathcal{E}_n^x, \mathcal{E}_n^y$ denote their respective x - and y -coordinates), while the denominator represents the time interval between these two events. The final velocity magnitude is normalized using Min-Max Normalization. Then, we define the spatial diffusion and temporal diffusion matrix of events' gradient, which includes spatial weight \mathcal{W}_s and temporal motion weight \mathcal{W}_t . Both weights are formulated based on exponential decay mechanisms, which can effectively convert physical features (distance \mathcal{D} and velocity \mathcal{V}) into interpretable weights ranging from 0 to 1, with the mathematical expressions as follows:

$$\mathcal{W}_s = \exp\left(-\frac{\mathcal{D}}{\sigma_s}\right), \quad \mathcal{W}_t = \exp\left(-\frac{\mathcal{V}}{\sigma_t}\right), \quad (10)$$

where σ_s and σ_t represent the variation of the spatio-temporal diffusion intensity. Finally, we obtain the final perturbation through the diffusion of the initial perturbation. We index the perturbation values of the temporal neighbors and spatial neighbors in the perturbation and multiply them by the corresponding diffusion coefficients. The final perturbation is

derived from the weighted average of these values,

$$\mathcal{P}_i = \frac{\mathcal{P}_i(\mathcal{I}_s) \cdot \mathcal{W}_s + \mathcal{P}_i(\mathcal{I}_t) \cdot \mathcal{W}_t}{2}. \quad (11)$$

4.2 Sample-wise Learning Rate Adjustment

In iterative perturbation optimization, the learning rate plays a critical role in balancing two core objectives: maximizing the attack success rate by misleading the target model to make wrong predictions and minimizing the perturbation cost by ensuring the perturbation is within acceptable bounds. Traditional batch-wise learning rate strategies adopt a unified learning rate for all samples in a batch. This approach simplifies optimization but overlooks the inherent heterogeneity of individual samples, leading to suboptimal attack performance. To address these issues, we propose a sample-wise learning rate adjustment strategy that dynamically assigns an adaptive learning rate to each individual sample based on its intrinsic characteristics and real-time optimization status.

To implement the sample-wise learning rate in perturbation update, we extend the Adam optimizer [Kingma, 2014] to incorporate dynamic sample-level learning rates. The complete update rules are defined as follows:

$$m = \beta_1 \cdot m + (1 - \beta_1) \cdot \nabla \mathcal{P}, \quad (12)$$

$$v = \beta_2 \cdot v + (1 - \beta_2) \cdot (\nabla \mathcal{P})^2, \quad (13)$$

$$\hat{m} = \frac{m}{1 - \beta_1^i}, \quad \hat{v} = \frac{v}{1 - \beta_2^i}, \quad (14)$$

where m denotes the first-moment (mean) estimate of the gradient of perturbation \mathcal{P} , with β_1 being the exponential decay rate for the first-moment, and v represents the second-moment estimate of the gradient of \mathcal{P} , with β_2 serving as the exponential decay rate for the second-moment; \hat{m} and \hat{v} are the bias-corrected first and second-moment estimates respectively, where i is the current iteration step introduced to elim-

inate the initial bias of m and v . Subsequently, the learning rate adjustment rule is shown below:

$$\eta[k] = \begin{cases} \eta[k] \cdot (a \cdot s + b \cdot (1 - s)) & \text{if } i \equiv 0 \pmod{n}, \\ \eta[k] & \text{otherwise,} \end{cases} \quad (15)$$

where $\eta[k]$ denotes the sample-wise learning rate for the k -th batch sample, s is a binary indicator variable for the attack outcome of the current sample (1 for success and 0 for failure), a and b are scaling coefficients, with specific adaptive implications (a is typically tuned to a value between 0 and 1 for fine-grained adjustment during successful update phases, and b is set to a value greater than 1 to scale up the learning rate when the previous update step is deemed a failure), n is the update interval for dynamic learning rate adjustment, and the modulo operation (\pmod{n}) is used to trigger learning rate scaling every n iterations. Finally, the optimized perturbation is updated by following:

$$\mathcal{P} = \mathcal{P} - \eta \cdot \frac{\hat{m}}{\sqrt{\hat{v}} + \gamma}. \quad (16)$$

where γ (typically set to 10^{-8}) is a small constant introduced to ensure numerical stability and avoid division by zero.

4.3 Loss Function

To guide the adversarial perturbation generation, we leverage a composite loss function that combines untargeted adversarial logits loss and Chamfer distance loss, ensuring both successful attacks and minimal distortion of the original point cloud structure.

For the untargeted attack objective, we adopt an adversarial loss function based on logits to maximize the gap between the logit of the true class and the maximum logit of other classes, thereby misleading the model to misclassify the input point cloud. The loss is formally defined as:

$$\mathcal{L}_{\text{cls}} = \frac{1}{B} \sum_{b=1}^B \max \left(z_b(y) - \max_{Y \neq y} z_b(Y) + \kappa, 0 \right), \quad (17)$$

where B is the batch size, $z_b(y)$ is the logit of the ground-truth class y for the b -th sample, $\max_{Y \neq y} z_b(Y)$ denotes the maximum logit of non-ground-truth classes for the b -th sample, and $\kappa \geq 0$ is a margin hyperparameter for untargeted attack effectiveness.

For the distance objective, we adopt the Chamfer distance to measure the similarity between the original events and the attacked events, and the corresponding loss function is defined as:

$$\mathcal{L}_{\text{distance}} = \frac{1}{N} \sum_{n'=1}^N \min_{n \in [1, N]} \left\| \mathbf{e}'^{(b, n')} - \mathbf{e}^{(b, n)} \right\|_2, \quad (18)$$

where N is the number of events in both the original events \mathcal{E} and attacked events \mathcal{E}' , $\mathbf{e}^{(b, n)}$ and $\mathbf{e}'^{(b, n')}$ are the n -th and n' -th events of \mathcal{E} and \mathcal{E}' for the b -th sample, respectively, and $\|\cdot\|_2$ is the Euclidean distance. $\mathcal{L}_{\text{distance}}$ is the average minimum distance from \mathcal{E}' to \mathcal{E} .

Ultimately, these two losses are combined using a weighted sum with parameter λ , where λ is determined through an optimized binary search process, as formulated in Eq. (1) and (2).

5 Experiment

In this section, we systematically validate the effectiveness and robustness of the proposed MA-ADV framework through comprehensive experiments. The platform configuration comprises the following: CPU: AMD 7950x, GPU: RTX 4090, and Memory: 32GB.

5.1 Experimental Setup

Our experiments utilize three public event-based datasets: DVSGesture [Amir *et al.*, 2017], N-Caltech101 [Orchard *et al.*, 2015], and N-MNIST [Orchard *et al.*, 2015]. We also implement three victim point-based backbones: EventMamba [Ren *et al.*, 2025b], PointNet++ [Qi *et al.*, 2017b], and PointNet [Qi *et al.*, 2017a]. For models without publicly available pre-trained weights, we retrain them from scratch on the corresponding datasets to obtain the weights used for subsequent attacks. Hyperparameter Settings: The total number of iterations I is set to 100, with a binary step J of 20. The initial learning rate η is configured as 1e-2. The λ_l and λ_h are set to 10 and 80, respectively. For the diffusion process, the KNN number K is 10, σ_s is 0.01, and σ_t is 0.1. The parameters a and b are set to 0.8 and 1.2.

5.2 Evaluation Metric

We assess the effectiveness of adversarial attacks using the attack Success Rate (SR), defined as the percentage of generated adversarial examples that successfully mislead the classifiers. Furthermore, we evaluate the distortion cost of generating these events using three metrics: Chamfer distance [Borgefors, 1986], Hausdorff distance [Huttenlocher *et al.*, 2002], and the L_2 norm distance [Goodfellow *et al.*, 2014].

5.3 Attack and Defend Method

We select five state-of-the-art point cloud adversarial attack methods as our baseline for comparison, including FGSM [Goodfellow *et al.*, 2014], IFGSM [Liu *et al.*, 2019], C&W + IFGSM [Xiang *et al.*, 2019], C&W [Xiang *et al.*, 2019], and HIT-ADV [Lou *et al.*, 2024]. To further assess the robustness of the proposed attack method under defensive settings, we also adopt three representative point cloud defense strategies, namely SOR [Rusu and Cousins, 2011], SRS [Lou *et al.*, 2024], and DUPNet [Zhou *et al.*, 2019].

5.4 Attack Results

Tab. 1 summarizes the comprehensive evaluation results of three point-based backbones across three datasets under six adversarial attacks. A clear trend emerges regarding the effectiveness of different attack strategies. Traditional gradient-based methods often result in significant perturbations to achieve high SR, whereas optimization-based attacks demonstrate superior efficiency by maintaining high attack success rates with minimal distortion. Specifically, our proposed MA-ADV consistently outperforms other baselines across all metrics. It achieves a perfect SR of 100% on all dataset combinations while simultaneously minimizing the Chamfer, L_2 , and Hausdorff distances. This indicates that MA-ADV can generate minimal-cost adversarial examples that are structurally very close to the original events.

Table 1: Performance metrics of three models under six adversarial attacks across DVSGESTURE, NCALTECH, and N-MNIST datasets. Specifically, the abbreviation "SR" denotes Success Rate, $\mathbb{D}_{\text{chamfer}}$ represents Chamfer Distance, \mathbb{D}_{L_2} is short for L_2 Distance, and $\mathbb{D}_{\text{hausdorff}}$ signifies Hausdorff Distance. A higher value of SR indicates better performance, whereas smaller values for the distance metrics are preferred.

Dataset	Method	EventMamba [Ren <i>et al.</i> , 2025b]				PointNet++ [Qi <i>et al.</i> , 2017b]				PointNet [Qi <i>et al.</i> , 2017a]			
		SR \uparrow	$\mathbb{D}_{\text{chamfer}} \downarrow$	$\mathbb{D}_{L_2} \downarrow$	$\mathbb{D}_{\text{hausdorff}} \downarrow$	SR \uparrow	$\mathbb{D}_{\text{chamfer}} \downarrow$	$\mathbb{D}_{L_2} \downarrow$	$\mathbb{D}_{\text{hausdorff}} \downarrow$	SR \uparrow	$\mathbb{D}_{\text{chamfer}} \downarrow$	$\mathbb{D}_{L_2} \downarrow$	$\mathbb{D}_{\text{hausdorff}} \downarrow$
DVSGESTURE	FGSM	0.9414	586.4739	44.4908	622.5184	0.9416	562.4741	43.4647	591.9448	0.8927	271.5300	28.7187	291.2435
	IFGSM	0.8861	12.4718	6.0955	14.6677	0.9821	8.4882	5.0408	9.9522	0.9964	2.5768	2.7606	2.7778
	C&W+IFGSM	1.0000	47.0102	10.4387	51.7008	1.0000	23.7156	5.8431	25.9396	1.0000	1.9981	1.2405	2.1329
	HIT-ADV	0.9138	23.7160	8.3958	51.1839	0.3485	2.6965	1.3618	4.7861	1.0000	0.9901	1.4419	2.3183
	C&W	0.9977	0.6918	1.1108	0.7768	1.0000	0.5128	0.6857	0.5568	0.9997	0.0071	0.0918	0.0093
	MA-ADV	1.0000	0.5598	1.0039	0.6487	1.0000	0.4296	0.3424	0.4742	1.0000	0.0051	0.0873	0.0068
NCALTECH	FGSM	0.9842	4370.4712	117.3863	4520.8867	0.7101	3628.3810	104.9289	3754.9340	0.9966	686.8976	45.3256	722.1955
	IFGSM	1.0000	66.9296	14.1339	82.4724	1.0000	35.4557	10.2922	38.0626	0.9971	6.3906	4.3667	6.8347
	C&W+IFGSM	1.0000	3.1356	0.8328	3.2736	1.0000	23.0316	3.7536	24.2463	1.0000	1.3429	0.9301	1.4331
	HIT-ADV	1.0000	2.8815	1.2445	6.7086	0.8053	71.4359	8.2967	146.5294	1.0000	54.1854	11.0535	122.5644
	C&W	1.0000	0.1702	0.3437	0.2125	1.0000	0.5846	1.0079	0.7710	1.0000	0.0188	0.1544	0.0214
	MA-ADV	1.0000	0.1118	0.2432	0.1592	1.0000	0.1309	0.4427	0.1904	1.0000	0.0043	0.0753	0.0062
N-MNIST	FGSM	0.8754	2548.1030	88.1012	2651.1113	0.5592	1460.3000	65.6142	1551.9330	0.8962	494.7847	38.4355	521.2792
	IFGSM	0.9133	40.4138	10.9905	45.8823	0.9999	19.4687	7.6384	21.6056	0.9556	5.2205	3.9444	5.4968
	C&W+IFGSM	1.0000	179.2462	20.5694	193.2784	1.0000	209.3543	22.5049	225.3949	1.0000	16.5717	5.5445	17.0246
	HIT-ADV	0.9984	151.9679	22.7492	301.5391	0.2733	20.4784	4.7725	38.1601	1.0000	16.8697	6.5788	36.1422
	C&W	1.0000	2.4263	2.2715	2.8778	1.0000	1.1441	1.6471	1.3456	1.0000	0.0149	0.1949	0.0184
	MA-ADV	1.0000	2.1017	2.0378	2.4133	1.0000	0.6750	0.9272	0.8643	1.0000	0.0056	0.1199	0.0078

Further analysis of the results reveals notable differences in model robustness. PointNet is more susceptible to small perturbations, while EventMamba requires larger distortions to be misled. The consistency of MA-ADV’s performance across all settings highlights its ability to find optimal perturbation directions that effectively exploit model vulnerabilities without introducing unnecessary structural changes. The minimal distance values achieved by MA-ADV across all datasets further confirm its efficiency and superiority over existing methods. Overall, the results demonstrate that MA-ADV maintains a strong balance between attack success and perturbation cost, making it a highly effective and practical adversarial attack method for event-based point cloud models. Furthermore, we visualize some adversarial examples generated from different methods in Fig. 3.

Additionally, we compare our method with the only two existing event attack methods. However, since neither provides a distance benchmark, our comparison is limited to the attack success rate. The authors of [Lee and Myung, 2022] achieved 97.74% on N-Caltech101 using shifting perturbation, whereas the work in [Büchel *et al.*, 2022] scored 99.88% on N-MNIST (lower than MA-ADV) and matched our 100% accuracy on DVSGesture.

5.5 Defense Results

Tab. 2 presents EventMamba’s performance under various defense strategies across three datasets. The results indicate that defenses can reduce attack effectiveness compared to the scenario without defense, but their impact varies significantly across datasets and attack methods. In general, MA-ADV

Table 2: EventMamba’s performance with different defense strategies on three datasets.

Dataset	Method	No Defense	SOR	SRS	DUP-Net
DVSGESTURE	C&W	0.9977	0.5442	0.4128	0.4183
	MA-ADV	1.0000	0.6187	0.4277	0.4108
NCALTECH	C&W	1.0000	0.302	0.1531	0.3004
	MA-ADV	1.0000	0.3709	0.1638	0.3145
N-MNIST	C&W	1.0000	0.2864	0.4259	0.4333
	MA-ADV	1.0000	0.4598	0.4701	0.4688

consistently achieves higher or comparable success rates relative to C&W across nearly all defense settings. This suggests that MA-ADV is more robust against common defenses and can better maintain its effectiveness even when models are protected. The performance gap between attacks also widens under certain defenses, highlighting the importance of considering defense mechanisms when evaluating adversarial attack methods. Overall, the results demonstrate that MA-ADV maintains strong performance in the presence of defenses, further validating its effectiveness and adaptability.

5.6 Ablation Study

Module Ablation: Tab. 3 presents the ablation study results for MA-ADV, where different components are systematically removed to evaluate their impact on attack performance. All variants maintain high attack success rates, and

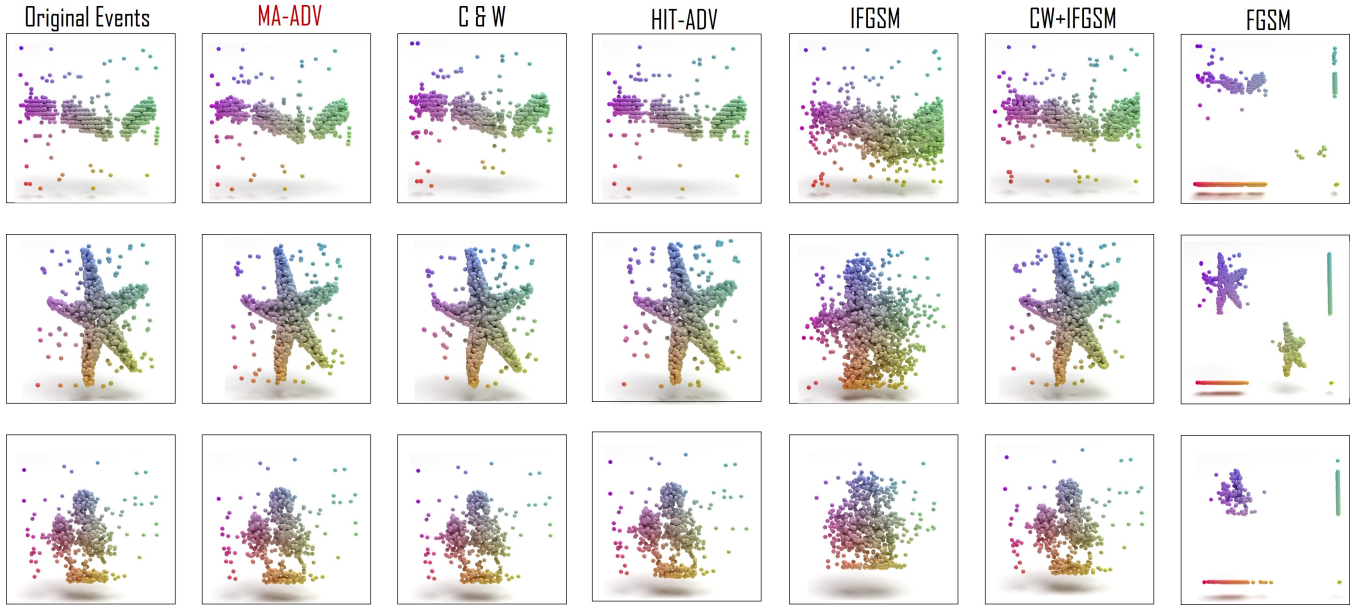


Figure 3: Visualization of adversarial event samples across different attack methods on three datasets. Zoom in find details.

Table 3: Ablation Study on Different Module Configurations.

Condition	SR \uparrow	$\mathbb{D}_{\text{chamfer}} \downarrow$	$\mathbb{D}_{L_2} \downarrow$	$\mathbb{D}_{\text{hausdorff}} \downarrow$
w/o Temporal	1.0000	0.6062	1.0384	0.6997
w/o Spatial	1.0000	0.6281	1.0563	0.7301
w/o Diffusion	0.9986	0.8049	1.1496	0.9089
w/o Adapter lr	0.9997	0.5497	1.0292	0.6359
w/o Causal	1.0000	0.5824	1.0332	0.6726
MA-ADV	1.0000	0.5598	1.0039	0.6487

most achieve a perfect SR of 100%, indicating that the overall attack framework remains effective even when individual components are omitted. However, the perturbation cost metrics reveal more distinct differences across configurations. Removing temporal diffusion or spatial diffusion leads to slight increases in Chamfer and Hausdorff distances, showing that both temporal and spatial consistency contribute to generating structurally similar adversarial events. The variant without the full diffusion process exhibits the largest increases in all distance metrics, which confirms that the diffusion mechanism plays a critical role in controlling perturbation magnitude and maintaining structural similarity. The variant without point-wise adaptive learning rate adjustment achieves smaller Chamfer and Hausdorff distances but fails to reach the optimal L_2 distance of the full model, suggesting that point-wise adaptive learning rates are particularly important for refining fine-grained perturbation scales. Removing causal information from temporal diffusion also results in slightly higher distance values, indicating that leveraging causal structures further improves perturbation efficiency. The full MA-ADV model, highlighted in gray, combines all

Table 4: Ablation Study on the number of diffusion point.

Number	SR \uparrow	$\mathbb{D}_{\text{chamfer}} \downarrow$	$\mathbb{D}_{L_2} \downarrow$	$\mathbb{D}_{\text{hausdorff}} \downarrow$
5	1.0000	0.6425	1.0711	0.7408
10	1.0000	0.5598	1.0039	0.6487
15	1.0000	0.5968	1.031	0.6921
20	1.0000	0.5862	1.0256	0.6809
25	0.9998	0.5807	1.0255	0.6745

components to achieve the best overall performance.

Diffusion Points Number Ablation: Tab. 4 shows the impact of varying the number of diffusion points on MA-ADV’s performance. All configurations maintain high success rates, and the model achieves a perfect SR when using 5 to 20 points. The results indicate that setting the number of diffusion points to 10 yields the best overall performance, with the lowest distances. Using fewer points (5) leads to larger perturbation costs, while increasing the number beyond 10 results in marginal improvements in distance metrics but no gain in attack success. When the number reaches 25, the success rate slightly decreases, suggesting that excessive diffusion steps may introduce unnecessary noise.

6 Conclusion

This paper proposes MA-ADV, a novel motion-aware framework for generating adversarial events via point cloud representations. By introducing a motion-aware perturbation diffusion strategy and a sample-wise learning rate adjustment mechanism, MA-ADV effectively mitigates high-frequency event noise and optimizes perturbation cost. Extensive experiments demonstrate the effectiveness and robustness of MA-ADV, highlighting its practicality in safety-critical scenarios.

References

[Amir *et al.*, 2017] Arnon Amir, Brian Taba, David Berg, Timothy Melano, Jeffrey McKinstry, Carmelo Di Nolfo, Tapan Nayak, Alexander Andreopoulos, Guillaume Garreau, Marcela Mendoza, et al. A low power, fully event-based gesture recognition system. In *Proceedings of the IEEE conference on computer vision and pattern recognition*, pages 7243–7252, 2017.

[Borgefors, 1986] Gunilla Borgefors. Distance transformations in digital images. *Computer vision, graphics, and image processing*, 34(3):344–371, 1986.

[Büchel *et al.*, 2022] Julian Büchel, Gregor Lenz, Yalun Hu, Sadique Sheik, and Martino Sorbaro. Adversarial attacks on spiking convolutional neural networks for event-based vision. *Frontiers in Neuroscience*, 16:1068193, 2022.

[Gallego *et al.*, 2020] Guillermo Gallego, Tobi Delbrück, Garrick Orchard, Chiara Bartolozzi, Brian Taba, Andrea Censi, Stefan Leutenegger, Andrew J Davison, Jörg Conradt, Kostas Daniilidis, et al. Event-based vision: A survey. *IEEE transactions on pattern analysis and machine intelligence*, 44(1):154–180, 2020.

[Goodfellow *et al.*, 2014] Ian J Goodfellow, Jonathon Shlens, and Christian Szegedy. Explaining and harnessing adversarial examples. *arXiv preprint arXiv:1412.6572*, 2014.

[Huang *et al.*, 2022] Qidong Huang, Xiaoyi Dong, Dongdong Chen, Hang Zhou, Weiming Zhang, and Nenghai Yu. Shape-invariant 3d adversarial point clouds. In *Proceedings of the IEEE/CVF conference on computer vision and pattern recognition*, pages 15335–15344, 2022.

[Huttenlocher *et al.*, 2002] Daniel P Huttenlocher, Gregory A. Klanderman, and William J Rucklidge. Comparing images using the hausdorff distance. *IEEE Transactions on pattern analysis and machine intelligence*, 15(9):850–863, 2002.

[Kingma, 2014] Diederik P Kingma. Adam: A method for stochastic optimization. *arXiv preprint arXiv:1412.6980*, 2014.

[Kurakin *et al.*, 2018] Alexey Kurakin, Ian J Goodfellow, and Samy Bengio. Adversarial examples in the physical world. In *Artificial intelligence safety and security*, pages 99–112. Chapman and Hall/CRC, 2018.

[LeCun *et al.*, 2015] Yann LeCun, Yoshua Bengio, and Geoffrey Hinton. Deep learning. *nature*, 521(7553):436–444, 2015.

[Lee and Myung, 2022] Wooju Lee and Hyun Myung. Adversarial attack for asynchronous event-based data. In *Proceedings of the AAAI Conference on Artificial Intelligence*, volume 36, pages 1237–1244, 2022.

[Lin *et al.*, 2025] Guixu Lin, Muyao Niu, Qingtian Zhu, Zhengwei Yin, Zhuoxiao Li, Shengfeng He, and Yinqiang Zheng. Adversarial attacks on event-based pedestrian detectors: A physical approach. In *Proceedings of the AAAI Conference on Artificial Intelligence*, volume 39, pages 5227–5235, 2025.

[Liu *et al.*, 2019] Daniel Liu, Ronald Yu, and Hao Su. Extending adversarial attacks and defenses to deep 3d point cloud classifiers. In *2019 IEEE International Conference on Image Processing (ICIP)*, pages 2279–2283. IEEE, 2019.

[Lou *et al.*, 2024] Tianrui Lou, Xiaojun Jia, Jindong Gu, Li Liu, Siyuan Liang, Bangyan He, and Xiaochun Cao. Hide in thicket: Generating imperceptible and rational adversarial perturbations on 3d point clouds. In *Proceedings of the IEEE/CVF Conference on Computer Vision and Pattern Recognition*, pages 24326–24335, 2024.

[Orchard *et al.*, 2015] Garrick Orchard, Ajinkya Jayawant, Gregory K Cohen, and Nitish Thakor. Converting static image datasets to spiking neuromorphic datasets using saccades. *Frontiers in neuroscience*, 9:437, 2015.

[Qi *et al.*, 2017a] Charles R Qi, Hao Su, Kaichun Mo, and Leonidas J Guibas. Pointnet: Deep learning on point sets for 3d classification and segmentation. In *Proceedings of the IEEE conference on computer vision and pattern recognition*, pages 652–660, 2017.

[Qi *et al.*, 2017b] Charles Ruizhongtai Qi, Li Yi, Hao Su, and Leonidas J Guibas. Pointnet++: Deep hierarchical feature learning on point sets in a metric space. *Advances in neural information processing systems*, 30, 2017.

[Ren *et al.*, 2023] Hongwei Ren, Yue Zhou, Yulong Huang, Haotian Fu, Xiaopeng Lin, Jie Song, and Bojun Cheng. Spikepoint: An efficient point-based spiking neural network for event cameras action recognition. *arXiv preprint arXiv:2310.07189*, 2023.

[Ren *et al.*, 2025a] Hongwei Ren, Zhuo Li, Aiersi Tuerhong, Haobo Liu, Fei Liang, Yongxiang Feng, Wenhui Wang, Yaoyuan Wang, Ziyang Zhang, Weihua He, et al. E2b: A single modality point-based tracker with event cameras. In *2025 IEEE International Conference on Robotics and Automation (ICRA)*, pages 6461–6468. IEEE, 2025.

[Ren *et al.*, 2025b] Hongwei Ren, Yue Zhou, Jiadong Zhu, Xiaopeng Lin, Haotian Fu, Yulong Huang, Yuetong Fang, Fei Ma, Hao Yu, and Bojun Cheng. Rethinking efficient and effective point-based networks for event camera classification and regression. *IEEE Transactions on Pattern Analysis and Machine Intelligence*, 2025.

[Rusu and Cousins, 2011] Radu Bogdan Rusu and Steve Cousins. 3d is here: Point cloud library (pcl). In *2011 IEEE international conference on robotics and automation*, pages 1–4. IEEE, 2011.

[Tang *et al.*, 2023] Keke Tang, Jianpeng Wu, Weilong Peng, Yawen Shi, Peng Song, Zhaoquan Gu, Zhihong Tian, and Wenping Wang. Deep manifold attack on point clouds via parameter plane stretching. In *Proceedings of the AAAI Conference on Artificial Intelligence*, volume 37, pages 2420–2428, 2023.

[Tsai *et al.*, 2020] Tzungyu Tsai, Kaichen Yang, Tsung-Yi Ho, and Yier Jin. Robust adversarial objects against deep learning models. In *Proceedings of the AAAI Conference on Artificial Intelligence*, volume 34, pages 954–962, 2020.

[Wei *et al.*, 2025] Xuqin Wei, Shijun Zheng, and Lina Yang. Smokeattack: Physically-based adversarial smoke for lidar point cloud detectors. *Pattern Recognition*, page 112920, 2025.

[Wen *et al.*, 2020] Yuxin Wen, Jiehong Lin, Ke Chen, CL Philip Chen, and Kui Jia. Geometry-aware generation of adversarial point clouds. *IEEE Transactions on Pattern Analysis and Machine Intelligence*, 44(6):2984–2999, 2020.

[Xiang *et al.*, 2019] Chong Xiang, Charles R Qi, and Bo Li. Generating 3d adversarial point clouds. In *Proceedings of the IEEE/CVF conference on computer vision and pattern recognition*, pages 9136–9144, 2019.

[Zhang *et al.*, 2025] Chiyu Zhang, Lu Zhou, Xiaogang Xu, Jiafei Wu, and Zhe Liu. Adversarial attacks of vision tasks in the past 10 years: A survey. *ACM Computing Surveys*, 58(2):1–42, 2025.

[Zheng *et al.*, 2019] Tianhang Zheng, Changyou Chen, Jun-song Yuan, Bo Li, and Kui Ren. Pointcloud saliency maps. In *Proceedings of the IEEE/CVF international conference on computer vision*, pages 1598–1606, 2019.

[Zhou *et al.*, 2019] Hang Zhou, Kejiang Chen, Weiming Zhang, Han Fang, Wenbo Zhou, and Nenghai Yu. Dupnet: Denoiser and upsampler network for 3d adversarial point clouds defense. In *Proceedings of the IEEE/CVF international conference on computer vision*, pages 1961–1970, 2019.

[Zhu *et al.*, 2018] Alex Zihao Zhu, Liangzhe Yuan, Kenneth Chaney, and Kostas Daniilidis. Ev-flownet: Self-supervised optical flow estimation for event-based cameras. *arXiv preprint arXiv:1802.06898*, 2018.